Electronic Supplementary Material (ESI) for Materials Chemistry Frontiers.

Supporting Information

Continuous impinging in a Two-stage Micromixer for the Homogeneous Growth of Monodispersed Ultrasmall Ni-Co Oxide on Graphene Flakes with Enhanced Supercapacitive Performance

Junping Zhao,[a] Yechao Wu,[a] Yihuang Chen,[a,b] Huile Jin,[a,b] Shuang Pan,[a] Shiqiang Zhao,[a] Xin Feng,[a,b] Yahui Wang,[a] Qingcheng Zhang[a,b*] and Shun Wang[a,b*]

[a]College of Chemistry and Materials Engineering, Wenzhou University, Zhejiang 325035, China

[b]Institute of New Materials and Industrial Technology, Wenzhou University, Wenzhou, Zhejiang, China

[*]Corresponding authors E-mail: zhangqc@wzu.edu.cn, shunwang@wzu.edu.cn

Fig. S1. The serious coagulation of Ni^{2+}/Co^{2+}/GO mixture.

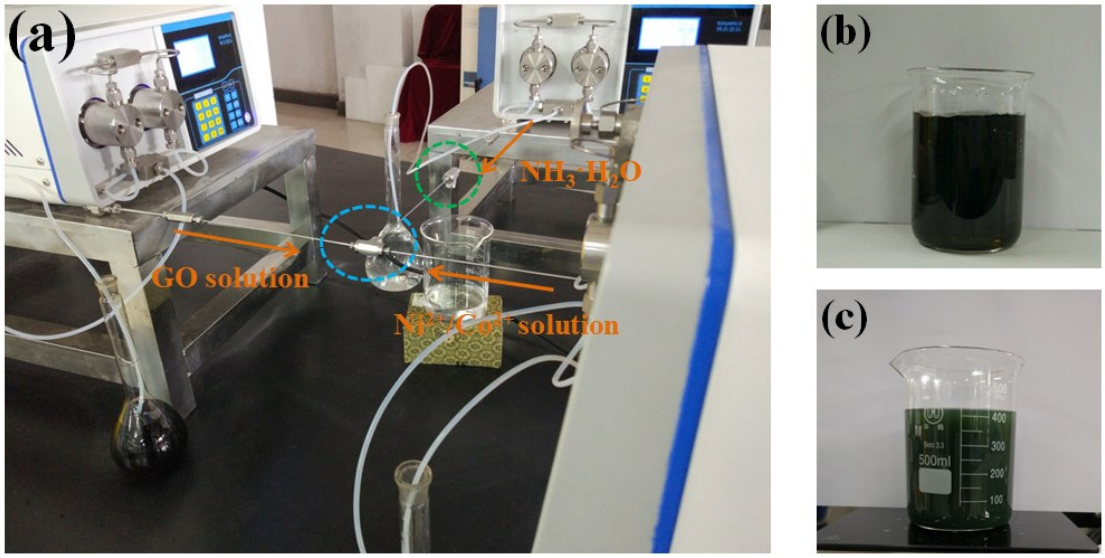

Fig. S2 (a) Synthesis of NCG-MM precursor in TS-MISR; (b) the homogeneous M^{2+}/GO mixture from the first T-junction outlet; (c) the precipitate solution from the second T-junction outlet.

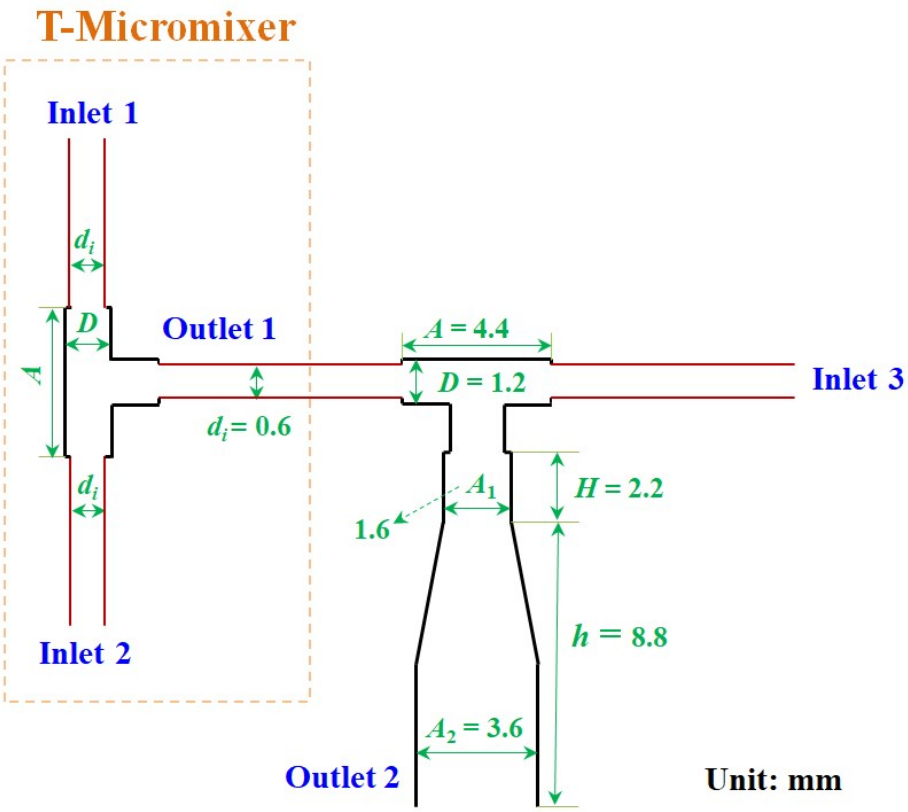

Fig. S3. Geometric structure of TS-MISR

Table S1. Premixing and Precipitation conditions of different NCG composites

Samples	Premixing	Precipitation	V_{A1}	V_{A2}	V_{A3}
NCG-MM	T-micromixer	MISR	80	80	160
NCG-MS	T-micromixer	STR	80	80	—
NCG-SM	STR	MISR	—	160	160
NCG-SS	STR	STR	—	—	—
NCG-MM-2	T-micromixer	MISR	40	40	80
NCG-MM-3	T-micromixer	MISR	60	60	120
NCG-MM-4	T-micromixer	MISR	100	100	200

[a] Unit of V_A: mL min^{-1}

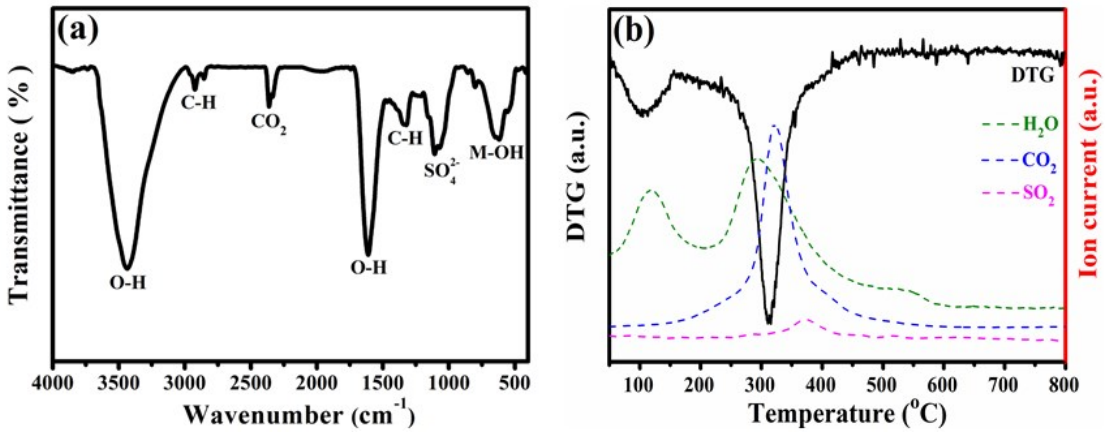

Fig. S4. (a) FT-IR spectrum and (b) TG-MS curves of NCG-MM precursor.

FT-IR technique was conducted to determine the molecular vibrations of anions presented in NCG-MM precursor, as shown in Fig. S4a. A broad band at around 3437 cm^{-1} was ascribed to the O-H stretching vibration of water molecules or OH^- groups presented in the framework layer to balance the positively charged Ni^{2+}/Co^{2+}, while the absorption band around 1630 cm^{-1} was assigned to the O-H bending vibration of absorbed water molecules. Two distinct peaks appeared at around 2358 and 1107 cm^{-1} suggested the existence of absorbed CO_2 and residual SO_4^{2-} intercalated in the α-phase $Ni_xCo_y(OH)_2$/RGO framework layers, respectively.[1] In addition, the weak bands around 2923 and 1327 cm^{-1} could be attributed to the C-H stretching vibration and C-H bending vibration of RGO flakes, respectively, while the characteristic bands in the region of 650-500 cm^{-1} were originated from the M-OH (M=Ni/Co) vibrations.[2]

The thermal behavior of NCG-MM precursor was evaluated by thermogravimetric analysis coupled with mass spectrometry, as shown in Fig. S4b. The NCG-MM precursor underwent two endothermic peaks when processed upon heating in the Ar flow. The first desorption peak located at around 100 °C was mainly due to the coincident evolution of physically absorbed H_2O and CO_2 in the

$Ni_xCo_y(OH)_2$/RGO structure, whereas the second weight loss appeared in the temperature range of 200–500 °C could be attributed to the pyrolysis of $Ni_xCo_y(OH)_2$ and labile oxygen-containing functional groups.[3] Therefore, some stable oxygen-containing functionalities that were not removed by *L*-ascorbic acid could be further eliminated under the thermal reduction. Besides, the evolution of SO_2 at 380 °C was derived from the decomposition of intercalated SO_4^{2-}. Therefore, the NCG-MM precursor should be SO_4^{2-} intercalated α-$Ni_xCo_y(OH)_2$/RGO flakes. [1]

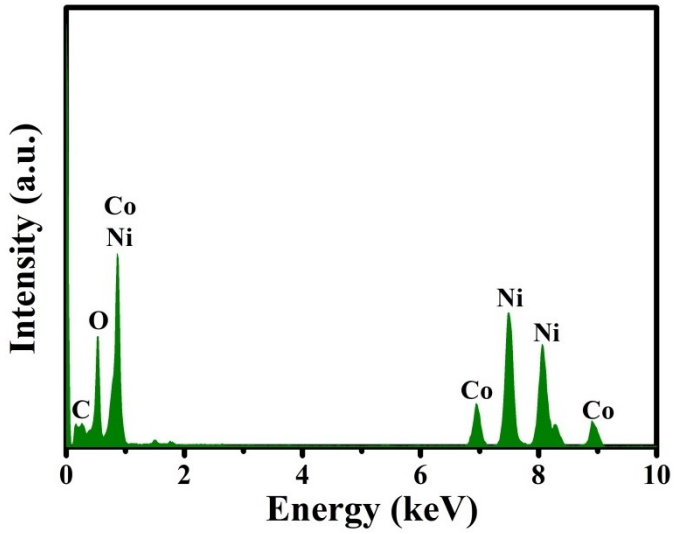

Fig. S5. EDS spectrum of NCG-MM

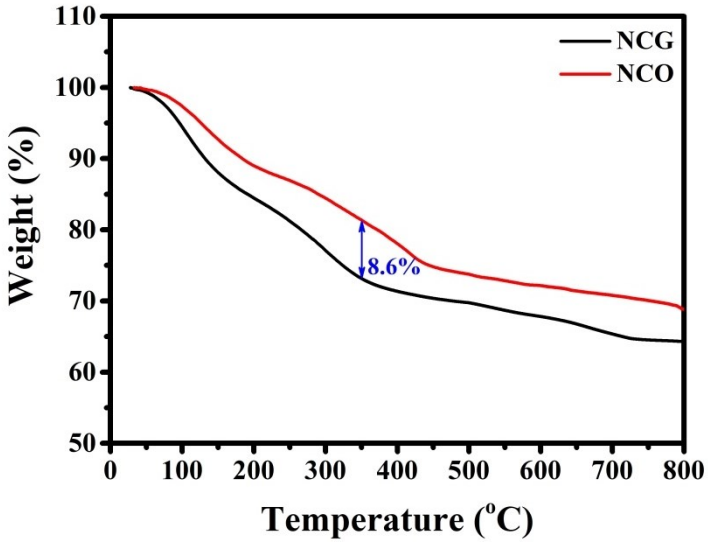

Fig. S6. TG curves of NCG and NCO treated in air

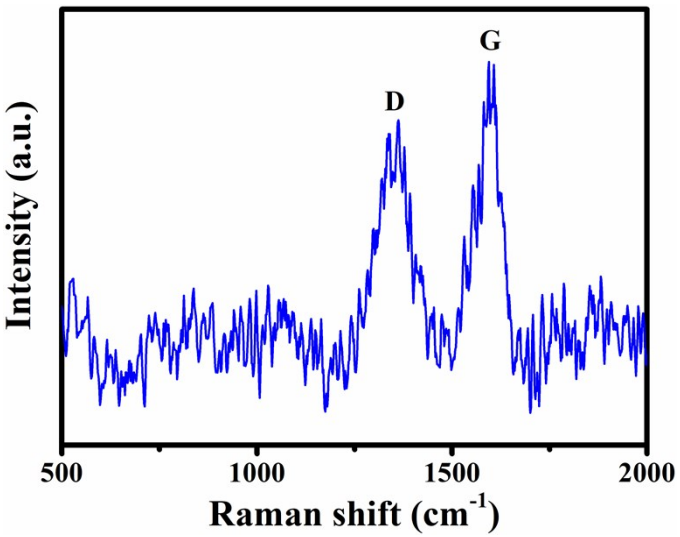

Fig. S7. Raman spectrum of $Ni_xCo_y(OH)_2$/GO

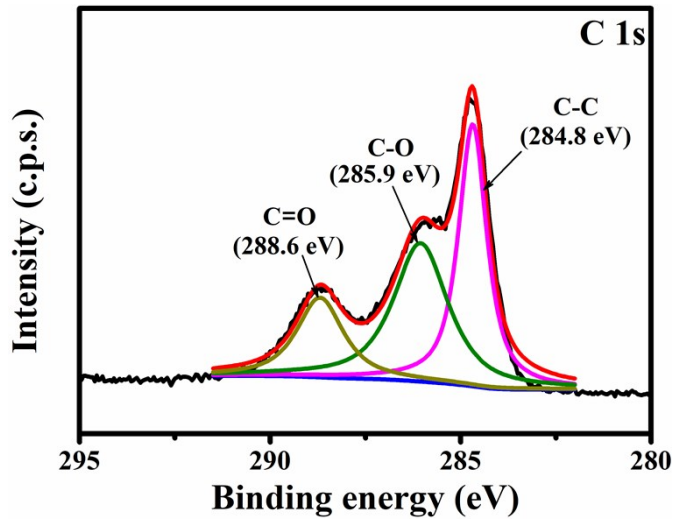

Fig. S8. High-resolution C 1s of $Ni_xCo_y(OH)_2$/GO

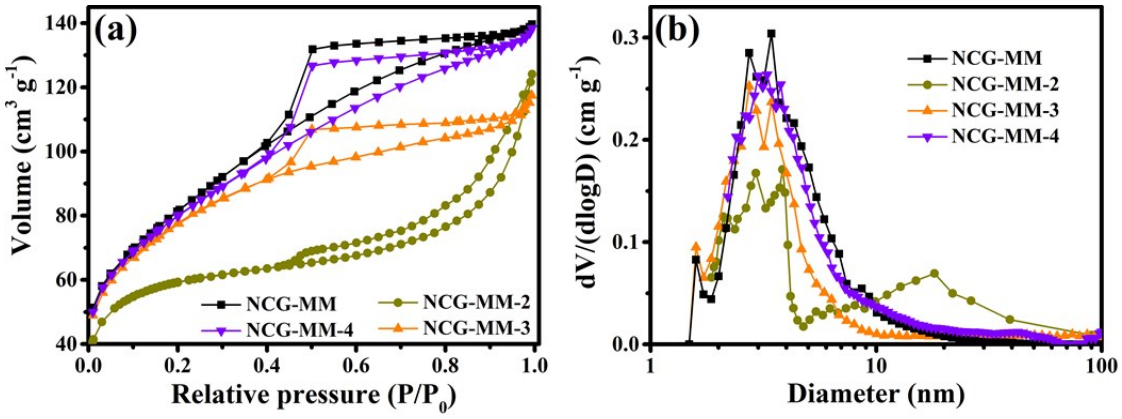

Fig. S9. (a) N_2 adsorption/desorption isotherms, (b) the particle size distribution of NCG composites synthesized at different volumetric flows in TS-MISR.

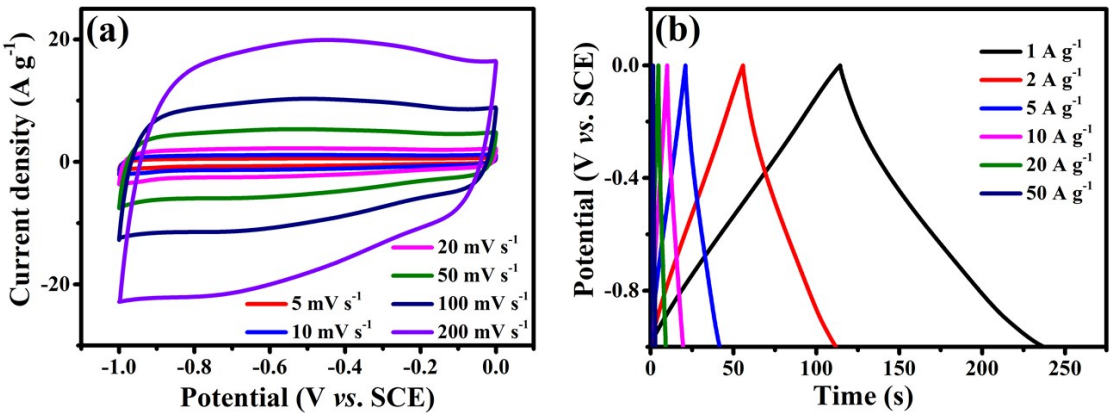

Fig. S10. (a) CV curves of RGO at various scan rates; (b) GCD curves of RGO at different current densities.

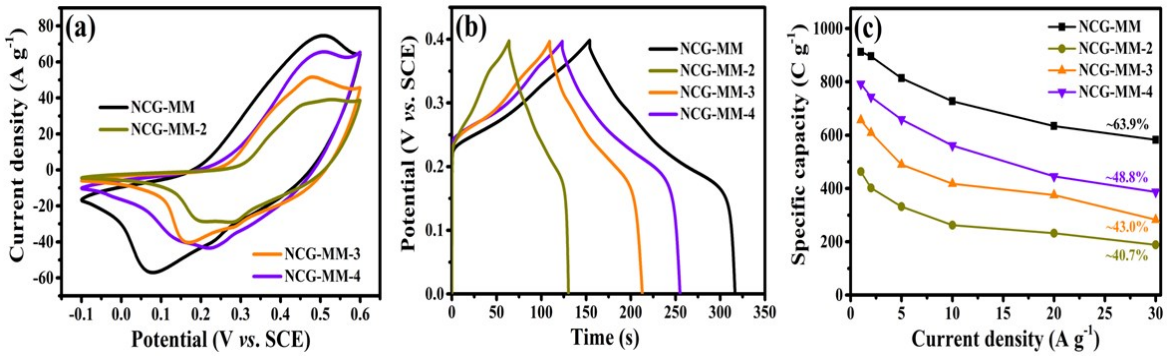

Fig. S11. (a) CV curves (50 mV s^{-1}), (b) GCD curves (5 A g^{-1}), (c) mass-specific capacitances of NCG composites synthesized at different V_A in TS-MISR.

Table S2. Comparison of the supercapacitive performances of Ni-Co-O/RGO synthesized in different methods

Materials	Synthetic methods	Specific capacitance ($F\ g^{-1}$)	Rate capability	Cycle Stability	Ref.
$NiCo_2O_4$/graphene	electrodeposition	1402 (1 A g^{-1})	77.0% (1→20 A g^{-1})	76.6% (5000)	4
$NiCo_2O_4$/RGO	electrodeposition	1392 (1 A g^{-1})	64.5% (1→30 A g^{-1})	80.0% (3000)	5
$NiCo_2O_4$/RGO	hydrothermal	947.4 (0.5 A g^{-1})	76.6% (0.5→10 A g^{-1})	97.9% (3000)	6
$NiCo_2O4$/RGO	hydrothermal	1003 (1 A g^{-1})	89.0% (1→10 A g^{-1})	57.0% (10000)	7
$NiCo_2O_4$/graphene	hydrothermal	2300 (1 A g^{-1})	30.9% (1→20 A g^{-1})	92.1% (4000)	8
$NiCo_2O_4$/N-RGO	solvothermal	2090 (1 A g^{-1})	60.1% (1→10 A g^{-1})	96.2% (5000)	9
$NiCo_2O_4$/RGO	spray drying	971 (0.5 A g^{-1})	20.8% (0.5→20 A g^{-1})	76% (5000)	10
$NiCo_2O_4$/3D RGO	template-assisted	708.4 (1 A g^{-1})	82.1% (1→16 A g^{-1})	94.3% (6000)	11
NiO@Co_3O_4 @RGO	MOF-derived	1361 (1 A g^{-1})	55.3% (1→30 A g^{-1})	76.4% (3000)	12
$NiCo_2O_4$/RGO	self- assembly	1388 (0.5 A g^{-1})	60.5% (0.5→30 A g^{-1})	90.2% (20000)	13
$NiMoO_4$/RGO	Microwave -assisted	1274 (1 A g^{-1})	44.9% (1→10 A g^{-1})	81.1% (1000)	14
$NiCo_2O_4$/RGO	self-combustion	1019 (1 A g^{-1})	66.1% (1→20 A g^{-1})	94.0% (2000)	15
Ni-Co-O/RGO	template-assistant precipitation (STR)	1211.2 (1 A g^{-1})	56.7% (1→10 A g^{-1})	90.5% (2000)	16
Ni-Co-O/RGO	precipitation (TS-MISR)	2281 (1 A g^{-1})	63.9% (1→30 A g^{-1})	94.3% (5000)	this work

References

1 F. Wang, X. Liu, F. Chen, H. Wan, Y. Lin, N. Zhang and R. Ma, Advanced supercapacitors based on α-$Ni(OH)_2$ nanoplates/graphene composite electrodes with high energy and power density, *ACS Appl. Energy Mater.*, 2018, **1**, 1496-1505.

2 J. Yang, C. Yu, C. Hu, M. Wang, S. Li, H. Huang, K. Bustillo, X. Han, C. Zhao, W. Guo, Z. Zeng, H. Zheng and J. Qiu, Surface-confined fabrication of ultrathin nickel cobalt-layered double hydroxide nanosheets for high-performance supercapacitors, *Adv. Funct. Mater.*, 2018, **28**, 1803272.

3 R. Larciprete, S. Fabris, T. Sun, P. Lacovig, A. Baraldi and S. Lizzit, Dual path mechanism in the thermal reduction of graphene oxide, *J. Am. Chem. Soc.*, 2011, **133**, 17315-17321.

4 Kuila, Tapas, Kim, N. Hoon, Lee, S. Hee, Zhang, Chunfei and J. Hee, Facile preparation of flower-like $NiCo_2O_4$/three dimensional graphene foam hybrid for high performance supercapacitor electrodes, *Carbon*, 2015, **89**, 328-339.

5 A. Rashti, B. Wang, E. Hassani, F. Feyzbar-Khalkhali-Nejad and T. S. Oh, Electrophoretic deposition of nickel cobaltite/polyaniline/rGO composite electrode for high-performance all-solid-state asymmetric supercapacitors, *Energy Fuels*, 2020, **34**, 6448-6461.

6 L. Ma, X. Shen, H. Zhou, Z. Ji, K. Chen and G. Zhu, High performance supercapacitor electrode materials based on porous $NiCo_2O_4$ hexagonal nanoplates/reduced graphene oxide composites, *Chem. Eng. J.*, 2015, **262**, 980-988.

7 S. Zhang, H. Gao, J. Zhou, F. Jiang and Z. Zhang, Hydrothermal synthesis of reduced graphene oxide-modified $NiCo_2O_4$ nanowire arrays with enhanced reactivity for supercapacitors, *J. Alloys Compd.*, 2019, **792**, 474-480.

8 S. Sun, S. Wang, S. Li, Y. Li, Y. Zhang, J. Chen, Z. Zhang, S. Fang and P. Wang, Asymmetric supercapacitors based on a $NiCo_2O_4$/three dimensional graphene composite and three dimensional graphene with high energy density, *J. Mater. Chem. A*, 2016, **4**, 18646-18653.

9 C. Huang, Y. Ding, C. Hao, S. Zhou, X. Wang, H. Gao, L. Zhu and J. Wu, PVP-assisted growth of Ni-Co oxide on N-doped reduced graphene oxide with enhanced pseudocapacitive behavior, *Chem. Eng. J.*, 2019, **378**, 122202.

10 A. Mondal, S. Maiti, S. Mahanty and A. Baran Panda, Large-scale synthesis of porous $NiCo_2O_4$ and rGO–$NiCo_2O_4$ hollow-spheres with superior electrochemical performance as a faradaic electrode, *J. Mater. Chem. A*, 2017, **5**, 16854-16864.

11 Y. Zhou, Z. Huang, H. Liao, J. Li, H. Wang and Y. Wang, 3D porous graphene/$NiCo_2O_4$ hybrid film as an advanced electrode for supercapacitors, *Appl. Surf. Sci.*, 2020, **534**, 147598.

12 X. Yin, C. Zhi, W. Sun, L.-P. Lv and Y. Wang, Multilayer NiO@Co_3O_4@graphene quantum dots hollow spheres for high-performance lithium-ion batteries and supercapacitors, *J. Mater. Chem. A*, 2019, **7**, 7800-7814.

13 Q. Li, C. Lu, C. Chen, L. Xie, Y. Liu, Y. Li, Q. Kong and H. Wang, Layered $NiCo_2O_4$/reduced graphene oxide composite as an advanced electrode for supercapacitor, *Energy Storage Mater.*, 2017, **8**, 59-67.

14 T. Liu, H. Chai, D. Jia, Y. Su, T. Wang and W. Zhou, Rapid microwave-assisted synthesis of mesoporous $NiMoO_4$ nanorod/reduced graphene oxide composites for high-performance supercapacitors, *Electrochim. Acta*, 2015, **180**, 998-1006.

15 A. N. Naveen and S. Selladurai, Novel low temperature synthesis and electrochemical

characterization of mesoporous nickel cobaltite-reduced graphene oxide (RGO) composite for supercapacitor application, *Electrochim. Acta*, 2015, **173**, 290-301.

16 Y. Xu, L. Wang, P. Cao, C. Cai, Y. Fu and X. Ma, Mesoporous composite nickel cobalt oxide/graphene oxide synthesized via a template-assistant co-precipitation route as electrode material for supercapacitors, *J. Power Sources*, 2016, **306**, 742-752.